

# Is the Number of Giant Arcs in $\Lambda$ CDM Consistent With Observations?

Guo-Liang Li<sup>1</sup>, S. Miao<sup>2</sup>, Y. P. Jing<sup>1</sup>, M. Bartelmann<sup>3</sup>, X. Kang<sup>1</sup>, M. Meneghetti<sup>3</sup>

## ABSTRACT

We use high-resolution N-body simulations to study the cross-sections and the predicted number of giant arcs in the  $\Lambda$ CDM model. We find that the prediction is sensitive to the source redshift, in qualitative agreement with Wambsganss et al. (2004). However, their assumption that the length-to-width ratio of arcs can be approximated by the magnification appears invalid. The violation of this assumption lowers the lensing probability by a factor of  $\sim 10$ . Thus, our predicted rate of giant arcs appears lower than the observed rate, although the precise discrepancy is unclear due to uncertainties both in theory and observations.

Subject headings: cosmology: galaxy clusters { gravitational lensing

## 1. INTRODUCTION

The Cold Dark Matter (CDM) scenario is now the standard model for structure formation. The "concordance"  $\Lambda$ CDM model (e.g., Ostriker et al. 1995) is supported by many observations, in particular the large-scale structure of the universe (e.g. Jenkins et al. 1998; Peacock et al. 2001; Tegmark et al. 2004) and the cosmic microwave background (e.g., Spergel et al. 2003).

Giant arcs are formed when background galaxies are distorted into long arc-like shapes by the gravitational shear of intervening clusters of galaxies. They are among the most beautiful images on the sky (e.g., see the Hubble Space Telescope images of A 2218, Keib et al. 1996). As clusters of galaxies are the largest bound structures in the universe, they

---

<sup>1</sup>Shanghai Astronomical Observatory; the Partner Group of MPA, Nandan Road 80, Shanghai 200030, China; Email: (lgl, ypjing, kangx)@center.shao.ac.cn

<sup>2</sup>University of Manchester, Jodrell Bank Observatory, Macclesfield, Cheshire SK11 9DL, UK; Email: smao@jb.man.ac.uk

<sup>3</sup>Zentrum für Astronomie, IITA, Universität Heidelberg, Albert-Uberle-Str. 2, 69120 Heidelberg, Germany; Email: (mbartelmann, meneghetti)@ita.uni-heidelberg.de

are at the tail of the mass function of bound structures. The formation of giant arcs therefore critically depends on the abundance and density profiles of clusters. Observationally, the number of giant arcs was first estimated using the Einstein Medium-Sensitivity Survey (EMSS) by Gioia & Luppino (1994). The largest dedicated search for giant arcs in clusters was performed by Luppino et al. (1999) who found strong lensing in 8 of the 38 X-ray selected clusters. These fractions were confirmed by Zaritsky & Gonzalez (2003) using the Las Campanas Distant Cluster Survey and Gladders et al. (2003) using the Red Cluster Survey. Both of these recent studies show that giant arcs are quite common in clusters of galaxies.

Earlier predictions of giant arcs use simple spherical models (e.g., Wu & Hammer 1993). However, such models are clearly inadequate, as the ellipticities and substructures of clusters can enhance the lensing cross-section by a large factor (Bartelmann & Weiss 1994; Bartelmann, Steinmetz & Weiss 1995). More recently, Torri et al. (2004) studied the importance of mergers for arc statistics. Wu & Mao (1996) compared the arc statistics in the Einstein-de Sitter universe and  $\Lambda$ CDM using simple spherical cluster models. A much more realistic study was performed by Bartelmann et al. (1998, hereafter B98) who first pointed out that the number of giant arcs in the  $\Lambda$ CDM model appears to be below the observed rate in clusters by a factor of 5-10. Meneghetti et al. (2000) investigated the effects of cluster galaxies on arc statistics and found that cluster galaxies do not introduce perturbations strong enough to significantly change the number of giant arcs. Flores, Maller & Primack (2000) drew a similar conclusion. Meneghetti et al. (2003) further examined the effect of  $\Lambda$ CDM galaxies on the giant arcs and concluded they are insufficient to resolve the discrepancy. Oguri et al. (2003) examined the ability of triaxial models of dark matter haloes to form giant arcs. They concluded that an inner power-law profile of  $r^{-1.5}$  can reproduce the observed giant arcs, while the standard NFW profile (Navarro, Frenk, & White 1997) with an inner profile of  $r^{-1}$  is unable to match the observations. Bartelmann et al. (2003) and Meneghetti et al. (2004) studied the probability of the formation of giant arcs in galaxy clusters in different dark-energy cosmologies. But the effect is insufficient still. In an important paper, Wambsganss et al. (2004) pointed out the simple fact that the probability of high lensing magnifications is very sensitive to the assumed source redshift. For example, a source at  $z_s = 1.5$  has a factor of  $\sim 5$  higher optical depth than a source at redshift  $z_s = 1$ . As the redshift distribution for the background source population that forms arcs is not well known, this introduces an uncertainty in comparing the observations and predictions.

In this paper, we use high-resolution simulations to re-examine the predicted number of giant arcs and compare our predictions with observations. The outline of the paper is as follows. In §2, we discuss the numerical simulations we use and the method we employ to identify giant arcs in simulated clusters. In §3, we present the main results of the paper. In particular, we confirm the results of Wambsganss et al. (2004; see also Dale et al. 2004) that

the predicted arc number is sensitive to the assumed source redshift distribution. However, we find that their assumption that the length-to-width ( $L=W$ ) ratio is equal to the absolute magnification appears to be invalid. This assumption was adopted in order to calculate the arc cross-section more efficiently as realistic modeling of the  $L=W$  ratio is quite time-consuming. We find, however, that ray-tracing simulations reduce the number of arcs by a factor of  $\sim 10$ . This reduction spoils the concordance found by Wambsganss et al. (2004) between the observations and predictions. We finish our paper with a discussion in §4.

## 2. Methods

### 2.1. Numerical Simulations

The cosmological model considered here is the current popular  $\Lambda$ CDM model with the matter-density parameter  $\Omega_m = 0.3$  and the cosmological constant  $\Omega_\Lambda = 0.7$  ( $\Lambda$ CDM). The shape parameter  $\Omega_b h^2$  and the amplitude  $\sigma_8$  of the linear density power spectrum are taken to be 0.2 and 0.9, respectively, where  $h$  is the Hubble constant in units of  $100 \text{ km s}^{-1} \text{ Mpc}^{-1}$ . A cosmological  $N$ -body simulation with a box size  $L = 300h^{-1} \text{ Mpc}$ , which was generated with our vectorized-parallel  $P^3M$  code (Jing & Suto 2002; Jing 2002), is used in this paper. The simulation uses  $512^3$  particles, so the particle mass  $m_p$  is  $1.67 \times 10^9 h^{-1} M_\odot$ . The gravitational force is softened with the S2 form (Hockney & Eastwood 1981) with the softening parameter taken to be  $30h^{-1} \text{ kpc}$ . The simulation has similar mass and force resolutions as that used by B98, but our simulation volume is 8 times larger, and hence contains roughly a factor of 10 more clusters. Compared with the simulations of Wambsganss et al. (2004, hereafter W04), our resolutions are a factor of 6.6 lower in mass and a factor of 10 lower in the force softening. Since strong arcs are produced mostly at radii  $\lesssim 100h^{-1} \text{ kpc}$  in the lens plane, the resolutions are sufficient (see also Dalal et al. 2004). This is also supported by the comparison of our results with those of W04 which have much higher resolutions { our predicted number of giant arcs is in reasonable agreement with that of W04 if the arcs are identified with their method. Notice, however, that W04 used  $\sigma_8 = 0.95$ , slightly higher than our value ( $\sigma_8 = 0.9$ ). This will cause some differences in our predicted number of arcs; we will return to this point later in §3.3.

Dark matter halos are identified with the friends-of-friends (FOF) method using a linking length equal to 0.2 times the mean particle separation. The halo mass  $M_h$  is defined as the virial mass enclosed within the virial radius according to the spherical collapse model (Kitayama & Suto 1996; Bryan & Norman 1998; Jing & Suto 2002).

## 2.2. Lensing Notations

For convenience of later discussions, we outline the notations we will use in the paper. We denote the lensing potential as  $\psi$ . The lens mapping from the lens and source plane is given by

$$\vec{y} = \vec{x} - \vec{r}; \quad (1)$$

and the distortion of images is then described by the Jacobian

$$\frac{\partial y_i}{\partial x_j} = \begin{pmatrix} 1 & \psi_{11} & \psi_{12} \\ \psi_{21} & 1 & \psi_{22} \end{pmatrix}; \quad (2)$$

where  $(y_1; y_2)$  are the source positions in the source plane, and  $(x_1; x_2)$  are the image positions in the lens plane. The Jacobian matrix is given in terms of the lensing potential by the  $2 \times 2$  matrix on the right hand side, which involves second-order derivatives of  $\psi$  with respect to  $x_1$  and  $x_2$ . The eigenvalues of the Jacobian matrix are denoted as  $\mu_1$  and  $\mu_2$ . Without losing generality, we will assume  $|\mu_1| > |\mu_2|$ . The (signed) magnification is given by

$$\mu = \frac{1}{\mu_1 \mu_2}; \quad (3)$$

For an infinitesimal circular source, the length to width ratio is simply given by

$$\frac{L}{W} = \frac{|\mu_1 - \mu_2|}{|\mu_1 + \mu_2|} = \frac{|\mu_2|}{|\mu_1|}; \quad (4)$$

## 2.3. Lensing Simulations

The lensing properties of numerical clusters are studied using the ray-tracing technique (e.g., B98; W04). For the source population, we use redshifts ranging from 0.6 to 7 with a uniform interval of 0.4. To calculate the optical depth, we use ten outputs for the simulated box from redshift 0.1 to 1 with a step size of 0.1. For each redshift, we select the 200 most massive clusters of galaxies as lenses. Notice that this cluster sample is more than a factor ten larger than the sample used by Bartelmann et al. (1998) and Shirley & White (2004), although our redshift samplings are sparser than the most recent study of Torri et al. (2004). For each cluster, we use a side-length of two virial radii and a projection depth  $2r_{\text{vir}}$ . The surface densities are then calculated for three orthogonal projections using the SPH smoothing algorithm (Monaghan 1992) on a  $1024 \times 1024$  grid. Usually, the kernel size is taken to be  $30h^{-1} \text{ kpc}$  (comoving). If the particle number within the kernel is fewer than 32, then we double the kernel size until the particle number is larger than 32. However, for the high density regions, when the particle number is larger than 400 within the kernel,

then we only use the nearest 400 particles to estimate the density. In order to obtain the lensing potential, we also use a larger grid (2048 × 2048) centered on the smaller grid; the surface densities are padded with zeros for all the pixels outside the inner grid. The lensing potential is then obtained using the FFT method (B98). Notice that the larger grid is used to avoid aliasing problems due to periodic boundary conditions.

To perform efficient lensing simulations, we first identify regions of interest in the lens plane that have magnifications exceeding  $\mu_{\text{lit}} \geq 2.5$  and regions with  $\mu_{\text{lit}} < 0$ ; other regions are unlikely to produce giant arcs with  $L=W$  exceeding 7.5. Following B98, we assume the sources have an ellipticity (axial ratio) randomly distributed between 0.5 to 1. Each source has an area  $S_{\text{source}}$  equal to a circular source with radius of 0.5 arc seconds. To have sufficient numbers of pixels in one image, the resolution in the regions of interest is increased to 0.1 arc seconds (see below) so that for most images, there are at least  $n_s = \frac{0.5^2}{0.1^2} \approx 200$  pixels.

For the regions identified above, the 1024 × 1024 (coarse) grid does not provide sufficient resolution. To remedy this, we obtain the lensing potential on a finer grid with resolution of 0.1 arc seconds using cubic spline interpolation of the surrounding 14 × 14 coarse grid points. In the same step, we obtain the source position for each grid point, and the corresponding magnification and eigenvalues ( $\lambda_1$  and  $\lambda_2$ ).

Once we obtain the lens mapping for the regions of interest from the lens plane to the source plane, we locate the smallest rectangle with area  $S_{\text{box}}$  that contains all the mapped pixels in the source plane. We then put sources randomly in this rectangle and obtain their imaging properties. The mapped regions in the source plane usually have irregular shapes, so the rectangle will enclose not only the regions of interest but also some pixels that do not satisfy our selection criteria ( $\mu_{\text{lit}} \geq 2.5$  or  $\mu_{\text{lit}} < 0$ ). To avoid sources that straddle the boundary of regions of interest, we only analyse sources further if they contain at least  $n_s$  pixels. In order to sample the arc formation regions sufficiently, a large number of sources are placed randomly inside the regions of interest. The number we generate is given by  $n_{\text{source}} = 9S_{\text{box}}/S_{\text{source}}$ , where  $S_{\text{source}} = 0.5^2$  in square arc seconds, and usually we have  $n_{\text{source}} > 10^4$ .

For the pixels contained in a source inside the region of interest, we use the lens mapping already derived to obtain the corresponding image positions, and then use the friends-of-friends method to identify giant arcs. To obtain the  $L=W$  ratio, we assume giant arcs can be approximated as ellipses. Numerically we find this assumption to be valid for most of our giant arcs. However, some images are irregular and cannot be fit well by an ellipse. But such cases are rare and thus they will not affect the cross-section significantly. To calculate the  $L=W$  ratio, we first identify the center of a giant arc,  $x_{\text{center}}$ , then find the point  $x_1$  that is the

furthest from  $x_{\text{center}}$ , and finally the point  $x_2$  that is the furthest from  $x_1$ . We then fit an arc that passes through these three points. The length of the arc is taken to be twice the major axis length of the ellipse,  $a$ . The length of the minor axis is taken to be  $b = \sqrt{S_{\text{image}}/a}$ , where  $S_{\text{image}}$  is the area covered by the image. The  $L=W$  ratio is then simply given by  $a=b$ . This procedure is identical to the ellipse fitting method in B98.

In W04, the arc  $L=W$  ratio is approximated by the magnification. Thus in order to obtain the arc cross-sections, they need to calculate the magnification patterns on a grid in the source plane. In W04, each pixel has a size of 1.5 arc seconds. However, we find that this pixel size is too large for small clusters in our simulations, so we used a grid of 0.1 arc seconds for all clusters instead. We use the Newton-Raphson method to find the image position and its corresponding magnification and eigenvalues. When there are multiple image positions, we use only the largest magnification. In the following, we will study the validity of two approximate measures of  $L=W$ , namely the magnification,  $\mu$  and the ratio of the two eigenvalues,  $\mu_1 = \mu_2$ . Under these two approximations, we obtain two corresponding measures of cross-sections, which we will denote as  $\sigma_{\mu}$  and  $\sigma_{\mu_1 = \mu_2}$ . We will compare these two cross-sections with that obtained through rigorous image simulation,  $\sigma_{\text{sim}}$ . The corresponding optical depths can be obtained by integrating the cross-sections along the line of sight (cf. Eq. 7), and we will denote these as  $\tau_{\text{sim}}$ ,  $\tau_{\mu}$  and  $\tau_{\mu_1 = \mu_2}$ . W04 assumes that  $\tau_{\mu} \approx \tau_{\text{sim}}$ . As can be calculated much more efficiently, this offers a much faster way of evaluating the arc cross-sections. Unfortunately, we will show below that, for realistic clusters of galaxies, this assumption appears to be invalid. As a result, their cross-section and optical depth are over-estimated.

### 3. Results

#### 3.1. Caustics, magnifications and cross-sections

For illustrative purposes, Fig. 1 shows the lensing properties for the fifth most massive clusters in our simulations at redshift 0.3. The source is at redshift 1. The bottom right panel shows the critical curves and the caustics. This configuration is similar to what other authors found in numerically simulated clusters. The other three panels show the maps of  $\mu$ ,  $\mu_1 = \mu_2$  and  $\mu_1/\mu_2 = 1 = \mu_2/\mu_1$  in the source plane. Recall that we only consider regions where  $\mu > \mu_{\text{limit}} = 2.5$  or  $\mu < 0$ . In other regions, we set  $\mu$  and  $\mu_1 = \mu_2$  to unity, which are shown as the black region in the top left panel. The colour bars show the range of the quantities plotted in the maps. Pixels with values exceeding the maximum of the colour bar are set equal to the maximum in the maps. If we approximate the arc  $L=W$  ratio as either  $\mu$  or  $\mu_1 = \mu_2$ , a comparison between the top two panels clearly indicates that the

cross-section will be much larger than the cross-section for a given length-to-width ratio. This effect is illustrated further in the bottom left panel where we plot the map of  $\beta = (\lambda_1 = \lambda_2)$ . In most cases, especially for the high magnification regions where arcs are expected to form, this ratio is larger than 1, which indicates that for an infinitesimal circular source,  $\beta$  will over-estimate the  $L=W$  ratio. As a check of our lensing simulations, Fig. 2 shows the magnification probability distribution for the cluster shown in Fig. 1. Our results nicely reproduce the asymptotic relation  $p(> j) \propto j^{-2}$  expected from the fold caustics when  $\beta > 1$  (e.g., Schneider, Ehlers, & Falco 1992).

To understand why the approximation  $L=W = j$  appears to over-estimate the arc cross-section, we study a cluster with a generalized NFW profile (Navarro, Frenk & White 1997)

$$\rho(r) / r = (r + r_s)^{-3} ; \tag{5}$$

where  $r_s$  is the scale radius. The cluster is at redshift of 0.3 and its mass is  $10^{15} h^{-1} M_\odot$  and we take  $\beta = 1.5$ . The concentration parameter  $c = r_{vir} = r_s$  is taken to be 2.28 (Oguri 2002). The source redshift is taken to be unity. Fig. 3 shows the relation between  $\lambda_1$  and  $\lambda_2$  for the minimum, saddle and maximum images in the time delay surface. The tangential arcs are primarily formed by the minimum images while the radial arcs are formed by the maximum images. For an infinitesimal circular source, the  $L=W$  ratio is equal to  $j$  multiplied by  $\lambda_1^2$  (see Eq. 4). It is clear that for the minimum image, at high magnifications,  $\lambda_1 \approx 0.65$ , while for the maximum image,  $\lambda_1 \approx 1.3$ . As for high magnifications, the asymptotic cross-section follows the probability distribution  $p(> j) \propto j^{-2}$  (Schneider et al. 1992), the cross-sections for the tangential arcs therefore satisfy  $\lambda_1^4 \approx 0.18$ . Similarly, for the radial arcs, we have  $\lambda_1^4 \approx 2.9$ . As the tangential arc cross-sections usually dominate over the radial arc cross-sections, it follows that the  $L=W = j$  assumption will over-estimate the arc cross-sections by a factor of  $\lambda_1 = 0.18 = 5.6$ .

Fig. 4 shows the ratio of  $\beta_{sim}$  and  $\beta$  for giant arcs as a function of the length-to-width ratio ( $L=W$ ). Recall that  $\beta_{sim}$  is the cross-section calculated through ray-tracing simulations, while  $\beta$  is obtained assuming that the  $L=W$  ratio is equal to the magnification. The four thin solid lines are the results for four individual clusters. The thick line is the cross-section weighted average for the 200 most massive clusters. In the same plot, the result of the generalized NFW model discussed above is also indicated. Clearly, the assumption that  $L=W = j$  leads to an over-estimate of the cross-sections by a factor of 7 and 10 for  $L=W = 7.5$  and  $L=W = 10$ , respectively.

Fig. 5 shows the ratio of  $\beta_{sim}$  and  $\beta$ , where  $\beta$  is again the cross-section calculated assuming  $L=W$  to be equal to the ratio of the two eigenvalues.  $\beta_{sim} = \beta$  is in the range of 0.5-2 when  $L=W$  is in the range from 5-20. Thus,  $\beta_{sim}$  offers a much better approximation

for the arc cross-section than  $\sigma_{\text{arc}}$ , at least for our assumed elliptical sources. Notice that, in our data, the more massive a cluster is or the larger the caustics are, the higher  $\sigma_{\text{sim}} = \sigma_{\text{arc}} / \sigma_{\text{cross}}$  and  $\sigma_{\text{sim}} = \sigma_{\text{arc}} / \sigma_{\text{cross}}$  become. For a cluster at a given redshift, as the source redshift increases, the caustics become larger. As a result,  $\sigma_{\text{sim}} = \sigma_{\text{arc}} / \sigma_{\text{cross}}$  also increases. This is useful for understanding why  $\sigma_{\text{sim}} = \sigma_{\text{arc}} / \sigma_{\text{cross}}$  increases as the source redshift increases (cf. Fig. 6).

### 3.2. Optical depths

To compute the optical depth, we first calculate the average cross section per unit comoving volume:

$$\bar{\sigma}_i(z_l; z_s) = \frac{P_i(z_l; z_s)}{V}; \quad (6)$$

where  $P_i(z_l; z_s)$  is the average cross section of the three projections of the  $i$ -th cluster at redshift  $z_l$ ,  $z_s$  is the source redshift, and  $V$  is the comoving volume of the box adopted in our lensing simulations. The optical depth can then be calculated as:

$$\tau_i(z_s) = \frac{1}{4 D_s^2} \int_0^{z_s} dz (z; z_s) (1+z)^3 \frac{dV_p(z)}{dz}; \quad (7)$$

where  $D_s$  is the angular diameter distance to the source plane, and  $dV_p(z)$  is the proper volume of a spherical shell with redshift from  $z$  to  $z + dz$ .

### 3.3. Comparison with previous studies

Fig. 6 shows the optical depth as a function of the source redshift. We qualitatively confirm the results of W04 that the optical depth is sensitive to the source redshift. The optical depth for a source at  $z_s = 1.5$  is a factor of 5 higher than the optical depth for a source at  $z_s = 1$ . Furthermore, if we adopt the same assumption as W04 (i.e.,  $L=W = j$ ), then our results are within 25% of their values (shown as triangles) for a source at  $z_s = 1$ . However, the difference becomes larger for higher redshift sources, namely their optical depth increases much faster than ours as a function of the source redshift. In our simulations, the increase in the optical depth plateaus for a source with  $z_s > 2$ . Similar discrepancies with W04 were found by Dalal et al. (2004).

However, if we use our rigorous approach of determining the  $L=W$  value, then our optical depth is reduced by a factor of 10 for a source at redshift 1. This is a direct result of the smaller cross-sections as we have shown in Figs. 4-5. As the optical depth determined by



W 04 is comparable to the observed value, our lower value of optical depth therefore worsens the agreement between the observed and predicted rates of giant arcs.

The difference between different studies can also be partially explained by the different values of  $\theta_8$  used, the effect of matter along the line of sight, and whether the numerical simulations have sampled the cluster mass function at the high-mass tail sufficiently. One effect emphasized by W 04 is the effect of matter along the line of sight. To investigate the effect of matter distribution (e.g., filaments) surrounding the cluster, we increase the projection depth to  $20h^{-1}$  Mpc (comoving) and the lens size to  $4r_{vir}$ . We write the new optical depths as  $\tau_{sim 2}$ ,  $\tau_2$  and  $\tau_2$ . The previous optical depths, calculated using a cube of side length  $2r_{vir}$ , are denoted by  $\tau_{sim 1}$ ,  $\tau_1$ ,  $\tau_1$ . Clearly the matter distribution around the clusters increases the optical depth but the effect appears to be small ( $\sim 15\%$ ). Perhaps the enhancement due to objects along the line of sight is more important. It can also be seen that  $\tau$  agrees with  $\tau_{sim}$  well. Furthermore,  $\tau = \tau_{sim}$  decreases as the source redshift increases. This is because the caustics become larger as the source redshift increases (see the end of x3.1).

The  $\theta_8$  value adopted by W 04 (0.95) is slightly larger than our value (0.9). This may also partially contribute to the difference in our optical depths. Fig. 7 shows the mass function of haloes at redshift 0.3 predicted by the extended Press-Schechter formalism (e.g., Sheth & Toomre 2002 and references therein; Press & Schechter 1976), the difference at large masses is around 50% even for such a small difference in  $\theta_8$ . This will increase the number of giant arcs in W 04 compared with ours. For the normalization adopted by B 98 for one set of their simulation data ( $\theta_8 = 1:12$ ), the abundance of clusters is a factor of  $\sim 3$  higher for  $M > 10^5 M_\odot$ . This will substantially increase the predicted number of giant arcs.

Most of our conclusions agree with those of Dalal et al. (2004), who used numerically-simulated clusters from the G IF collaboration (Kaumann et al. 1999). Their mass and spatial resolutions are similar to ours. However, their overall optical depths are larger than ours by a factor of 6 for  $z_s = 1:0$ . The difference is partly due to the different definitions of the L=W ratio. Dalal et al. treat the giant arcs by a rectangle, rather than an ellipse as in our case. Thus for the same giant arc, the L=W ratio in Dalal et al. (2004) is equal to 4 times our L=W ratio. As a result, their optical depth for giant arcs with L=W  $\sim 10$  should be compared with our value for L=W  $\sim 7.5$ . For example, for  $z_s = 1:1.5$  and 2, our optical depths for giant arcs with L=W  $\sim 7.5$  (in our definition) are  $1:0 \times 10^7$ ;  $4:8 \times 10^7$  and  $1:0 \times 10^6$ , respectively. These should be compared with their corresponding values of  $2:5 \times 10^7$ ,  $7 \times 10^7$ , and  $1:4 \times 10^6$ . Our value is lower than theirs by about 40% for a source at redshift 1.5 and 2. But the discrepancy becomes larger for a source at redshift 1. At such low redshift, the cross-section is increasingly dominated by the few most massive

clusters as the critical surface density increases. So the cosmic variance becomes important, particularly for the G IF simulations which have a simulation volume 9.6 times smaller than ours. A detailed comparison between our numerical methods indicate that our cross-sections agree with each other within 25% for the same numerical cluster (with the same projection) selected from the G IF simulations (Dalal 2005, private communication)<sup>1</sup>. We believe the remaining difference is due to different mass functions in our simulations and the fact that Dalal et al. (2004) used more than three projections for the more massive clusters to calculate the cross-sections. Fig. 7 shows that the G IF mass function at large mass appears higher than ours. This will increase their optical depths for giant arcs and perhaps explain the remaining discrepancy.

#### 4. Discussion

In this paper we used numerically simulated clusters to study the arc rate in clusters of galaxies. We use a similar methodology as B98, but in our study the number of clusters is about a factor of ten higher than previous studies (e.g., B98 and Dalal et al. 2004). We calculated the cross section and optical depth for different ways to calculate the length-to-width ratio ( $L=W$ ) and as a function of the source redshift. Our results qualitatively confirm the conclusion of W04, that the strong-lensing optical depth is sensitive to the source redshift. However, we find that their assumption that the  $L=W$  ratio can be approximated by the magnification appears to over-estimate the number of giant arcs. We also examined the effect of the matter distribution around clusters. We find this increases the lensing cross-section slightly, by 15%. A multiple lens-plane lensing simulation is needed to investigate the effect of the objects along the line of sight but further away from the clusters, as done by W04. It is still a matter of debate how important this effect is (e.g., W04; Dalal et al. 2004).

Both W04 and Dalal et al. (2004) claim that the predicted and observed rates of giant arcs are consistent with each other. However, the conclusion of W04 is based on the assumption that the  $L=W$  ratio is equal to the magnification. We find this assumption invalid in practice and this violation substantially lowers the predicted rate of giant arcs. Our predicted rate of giant arcs with  $L=W = 7.5$  is lower by 40% than the value of Dalal et al. (2004) for a source at redshift 1.5 and 2.0. For a source at redshift 1, our prediction is lower than theirs by a factor of 2.5. We believe some of the differences are due to cosmic variance { the G IF simulation has a cosmic volume that is 9.6 times smaller than ours. Their mass

---

<sup>1</sup>We also compared two different numerical codes developed separately by us. The cross-sections from these two methods for the cluster shown in Fig. 1 agree within 10% -30% .

function appears to be somewhat higher than ours (see Fig. 7). In any case, the agreement between the observations and the predictions of Dala et al. (2004) also depends on whether the giant arcs can be modelled as rectangles rather than ellipses, as more commonly assumed.

We conclude that our predicted rate may be a factor of a few lower than the "observed" rate. However, it is unclear how serious this discrepancy is, as both observations and theoretical predictions are uncertain. Observationally, we need more transparent selection criteria (see Dala et al. 2004 for excellent discussions). Furthermore, the  $L=W$  determination from ground-based telescopes may be affected by seeing, leading to a likely underestimate of the  $L=W$  ratio as the widths of many arcs are unresolved. A reliable prediction of the giant arcs also requires the information of the source population as a function of magnitude, surface brightness and redshift, which is currently lacking.

Theoretically, we need higher resolution simulations in very large simulation boxes so that we can sample the cluster mass function and resolve the internal structure of clusters simultaneously. Numerical simulations with baryonic cooling and star formation will also be needed to make more detailed comparisons with observational data. While baryonic cooling is not expected to be very efficient in clusters of galaxies (most baryons in clusters are still in the hot phase seen as X-rays), nevertheless, its effects may not be negligible, particular for the giant arcs at small radii (Dala et al. 2004; see also Oguri 2003). In this regard, hydro-dynamical cosmological simulations also offer the possibility of a more direct comparison with observations, at least with the EMSS, as the X-ray luminosities of clusters of galaxies in these simulations can be predicted (with some uncertainty), and hence we can apply similar selection criteria for clusters of galaxies as in observations and examine the arc formation abilities of these X-ray clusters.

As many observations converge to the concordance cosmology, it will be interesting to use lensing to constrain parameters such as  $\Omega_8$  independently in the  $\Omega_0 = 0.3$ ;  $\Omega_0 = 0.7$  at cosmology. As the cluster mass function depends sensitively on  $\Omega_8$ , the arc statistics should provide a stringent limit on  $\Omega_8$ . This parameter is still somewhat uncertain: some studies prefer values as high as 1.1, while others prefer values as low as 0.7 (see Tegmark 2004 for a recent overview of current results). We plan to return to some of these issues in the future.

We thank Drs. L. Gao, W. P. Lin and in particular N. Dala for helpful discussions. YPJ is supported in part by NKBRSF (G19990754) and by NSFC. SM acknowledges the financial support of Chinese Academy of Sciences and the EU ANGLES research network.

REFERENCES

- Bartelmann, M., Huss, A., Colberg, J.M., Jenkins, A., Pearce, F.R. 1998, *A & A*, 330, 1 (B 98)
- Bartelmann, M., & Weiss, A. 1994, *A & A*, 284, 285
- Bartelmann, M., Steinetz, M. & Weiss, A. 1995, *A & A*, 297, 1
- Bartelmann, M.; Meneghetti, M.; Perrotta, F.; Baccigalupi, C.; Moscardini, L. 2003, *A & A*, 409, 449
- Bryan, Greg L.; Norman, Michael L. 1998, *ApJ*, 495, 80
- Dalal, N., Holder, G., Hennawi, J.F. 2004, *ApJ*, 609, 50
- Flores, R.A., Miller, A.H., Primack, J.R. 2000, *ApJ*, 535, 555
- Gioia, I.M., Luppino, G.A. 1994, *ApJS*, 94, 583
- Gadders, M.D., Hoekstra, H., Yee, H.K.C., Hall, Patrick, B., Barrientos, L.F. 2003, *ApJ*, 593, 48
- Hockney, R.W., Eastwood, J.W. 1981, *Computer Simulation Using Particles*, New York: McGraw-Hill, 1981
- Monaghan, J.J. 1992, *ARA & A*, 30, 543
- Jenkins, A. 1998, *ApJ*, 499, 20
- Jing, Y.P. 2000, *ApJ*, 535, 30
- Jing, Y.P. & Suto Y. 2002, *ApJ*, 574, 538
- Jing, Y.P. 2002, *MNRAS* 335, L89
- Kaumann G., Colberg, J.M., Diaferio, A., White, S.D.M. 1999, *MNRAS*, 303, 188-206,
- Kitayama, T., & Suto, Y. 1996, *MNRAS*, 280, 638
- Kneib, J.-P., Ellis, R.S., Smail, I., Couch, W.J., Sharples, R.M. 1996, *ApJ*, 471, 643
- Luppino, G.A., Gioia, I.M., Hammer, F., LeFevre, O., Annis, J.A., 1999, *A & AS*, 136, 117
- Meneghetti, M., Bolzonella, M., Bartelmann, M., Moscardini, L., Tomén, G.. 2000, *MNRAS*, 314, 338
- Meneghetti, M., Bartelmann, M., Moscardini, L. 2003, *MNRAS*, 346, 67
- Meneghetti, M., Bartelmann, M., Dolag, K., Moscardini, L., Perrotta, F., Baccigalupi, C., Tomén, G. 2004, *astro-ph/040570*
- Navarro, J.F., Frenk, C.S., White, S.D.M. 1997, *ApJ*, 490, 493
- Ostriker, J.P., & Steinhardt, P.J. 1995, *Nature*, 377, 600

- Oguri, M . 2002, *ApJ*, 573, 51
- Oguri, M ., Lee, J., Suto, Y . 2003, *ApJ*, 599, 7
- Peacock, J. A ., et al. 2001, *Nature*, 410, 169
- Press, W . H ., & Schechter, P . 1974, *ApJ*, 187, 425
- Schneider, P ., Ehlers, J., Falco, Emilio E . 1992, *Gravitational Lenses* (Springer Verlag: New York)
- Sheth, R . K ., Toomey, G . 2002, *MNRAS*, 349, 1464
- Shirley, H ., Martin, W . 2004, *astro-ph/0408245*
- Spergel, D . N . et al. 2003, *ApJS*, 148, 175
- Stoehr, F ., White, S . D . M ., Toomey, G ., Springel, V . 2002, *MNRAS*, 335, L84
- Tegmark, M . 2004, *ApJ*, 606, 702
- Tegmark, M . et al. 2004, *Phys. Rev. D*, 69, 103501
- Torri, E ., Meneghetti, M ., Bartelmann, M ., Moscardini, L ., Rasia, E ., Toomey, G . 2004, *MNRAS*, 349, 476
- Wambsganss, J., Bode, P., Ostriker, J. P., 2004, *ApJ*, 606, L93 (W 04)
- Wu, X .-P ., Hammer, F . 2003, *MNRAS*, 262, 187
- Wu, X .-P ., Mao, S . 1996, *ApJ*, 463, 404
- Zaritsky, D . & Gonzalez, A . H ., 2003, *ApJ*, 584, 691

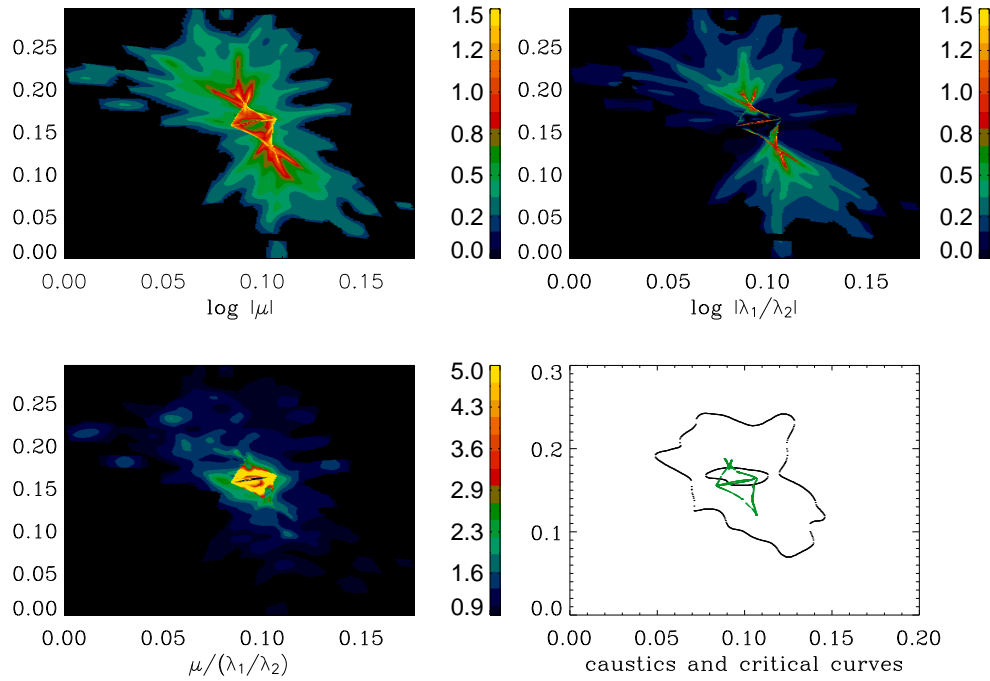


Fig. 1. | Maps of the absolute magnification (top left), ratio of the two eigenvalues  $\mu/(\lambda_1/\lambda_2)$  (top right),  $\mu/(\lambda_1/\lambda_2)$  (bottom left), and the caustics and critical curves (bottom right panel) are shown for one of our simulated clusters. The lengths in the four panels are all in units of  $h^{-1} \text{Mpc}$ . The  $\mu/(\lambda_1/\lambda_2)$  values in regions where  $0 < \mu/(\lambda_1/\lambda_2) < 2.5$  are set to unity. Pixels with values exceeding the maximum of the color bars are set equal to the maximum.

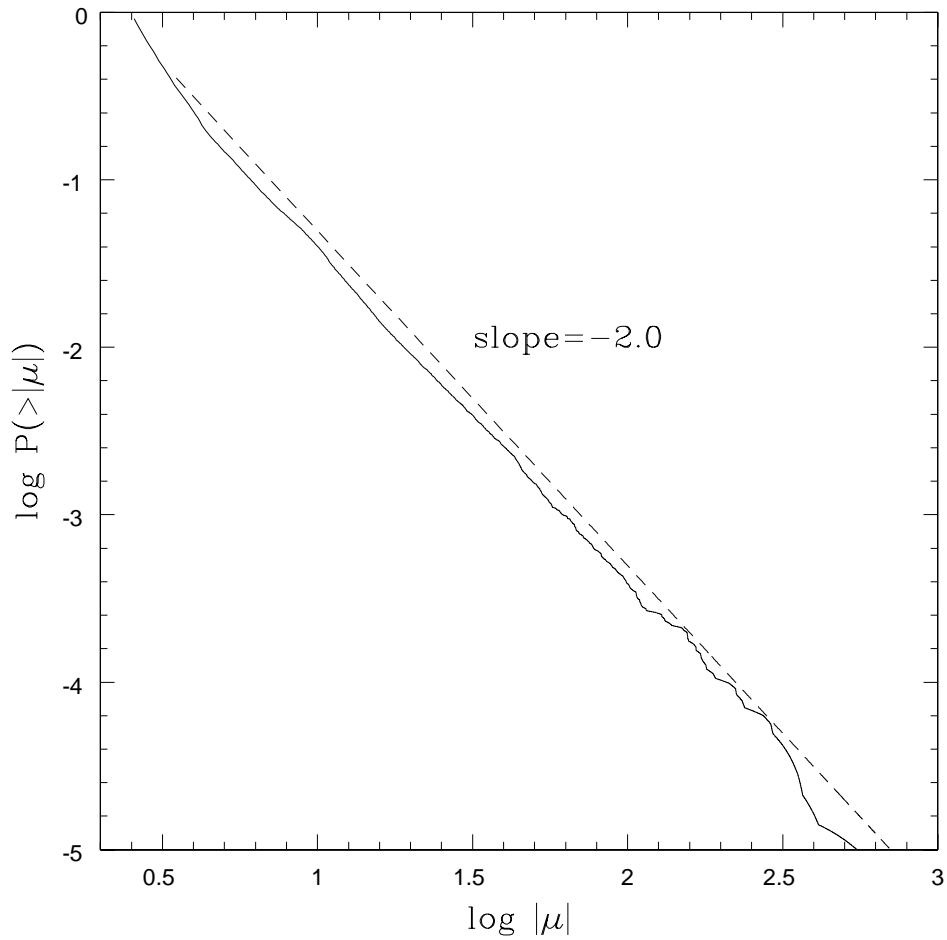


Fig. 2. The fraction of area in which the magnification is larger than a given  $|\mu|$  in the source plane. The data are taken from one realization of the projected surface density for the 5th most massive cluster (shown in Fig. 1). The behavior can be well fitted by the expected asymptotic power-law,  $P(>|\mu|) \propto |\mu|^{-2}$ , as indicated by the dashed line.

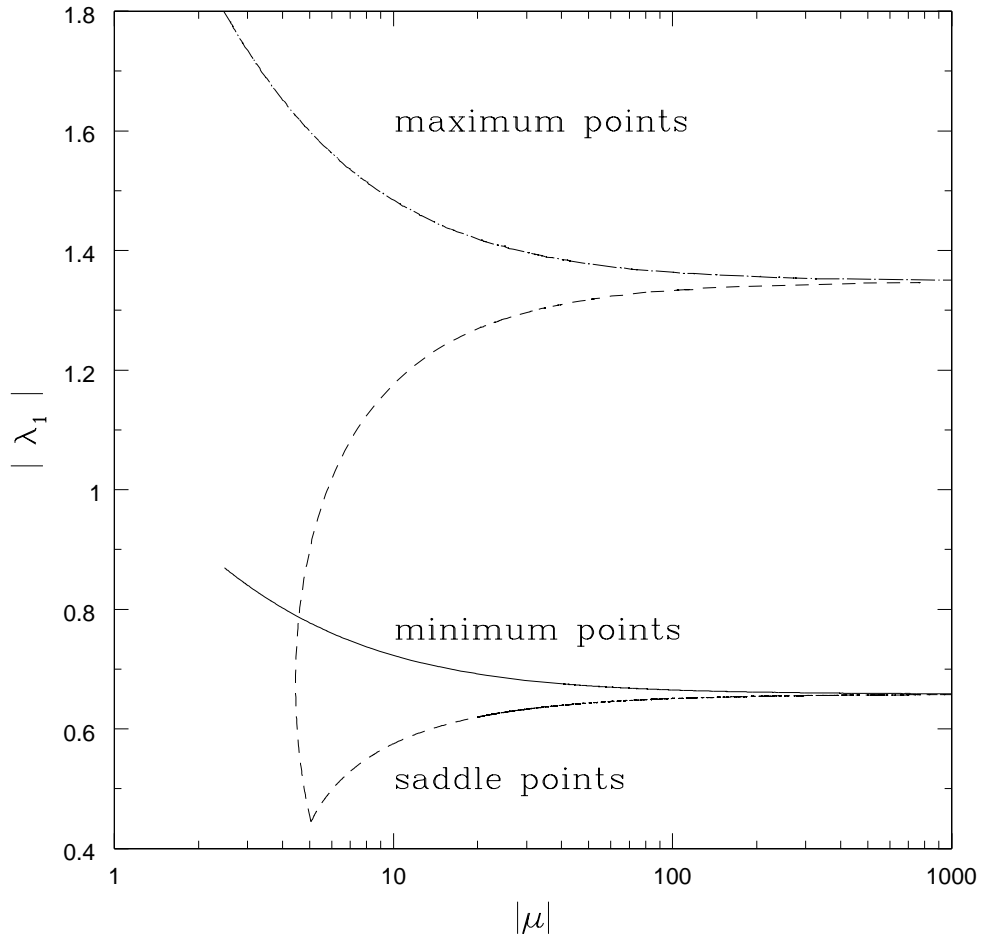


Fig. 3. | Magnification  $j$  vs. the larger of the two eigenvalues for a cluster described by a generalized NFW model (eq. 5) with  $\beta = 1.5$  and a total mass of  $M = 10^{15} h^{-1} M_{\odot}$ . The solid, dashed, and dot-dashed lines are for the minimum, saddle and maximum images in the time delay surface, respectively. For an infinitesimal source,  $j = \frac{4}{3}$  for large magnifications (see the text).



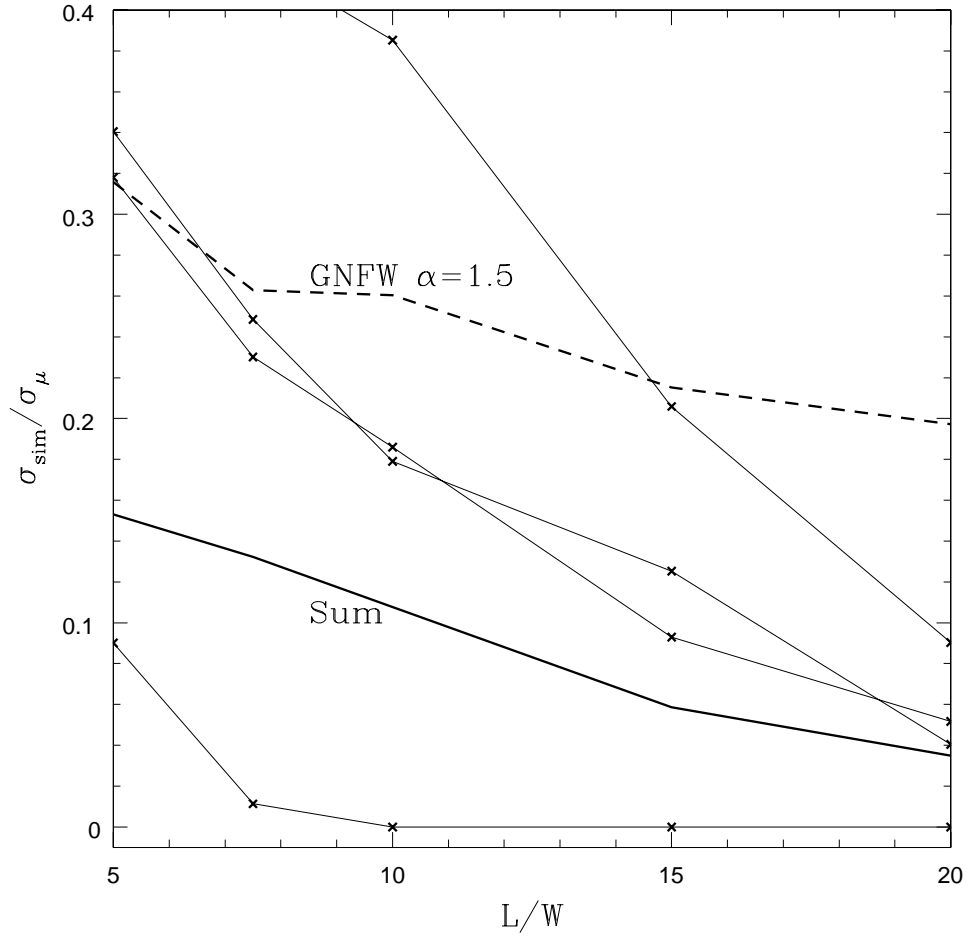


Fig. 4. | The ratio of the cross-sections  $\sigma_{sim}$  and  $\sigma_{\mu}$ , where  $\sigma_{sim}$  is calculated through detailed simulations using ray tracing, while  $\sigma_{\mu}$  is calculated assuming the  $L=W$  ratio is equal to the magnification. The solid lines are the results for four individual clusters while the dashed line is for our generalized NFW model. The thick line is the cross-section weighted average for the 200 most massive clusters in our simulations. The lens and source redshifts are taken to be  $z_1 = 0.3$  and  $z_s = 1.0$ , respectively.

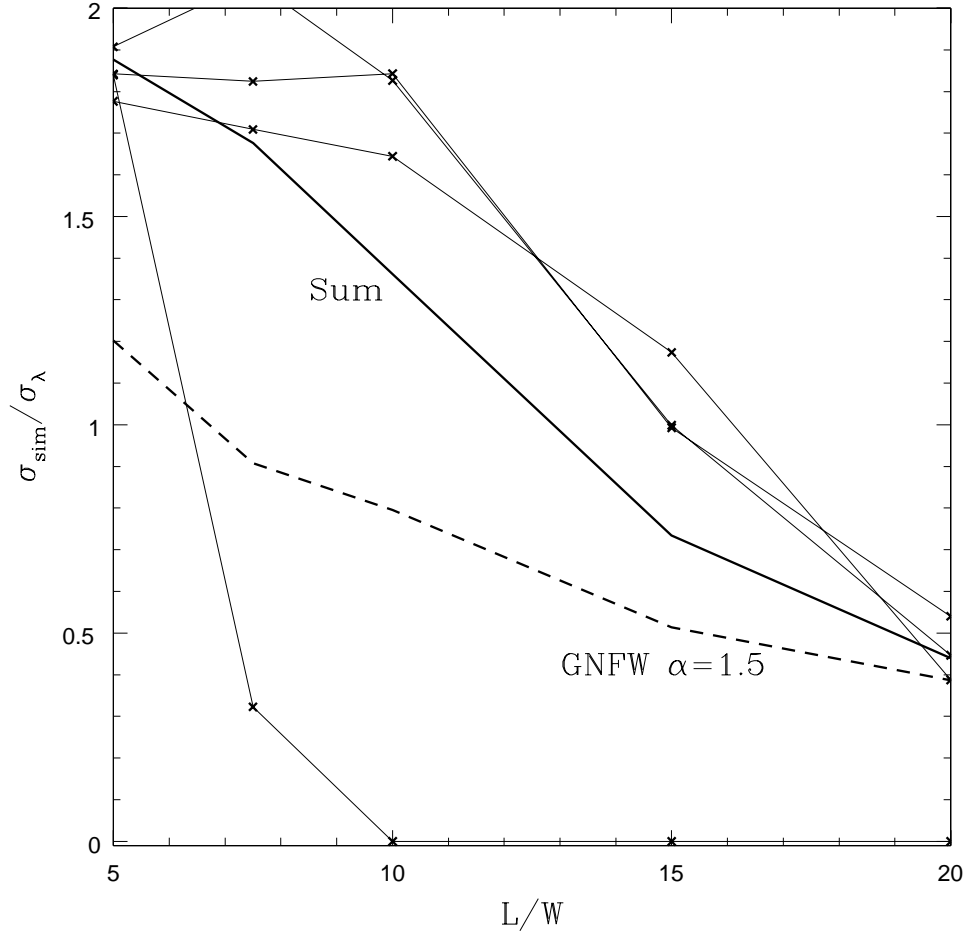


Fig. 5. | The ratio of the cross-sections where the  $L=W$  ratio is obtained through ray-tracing and under the assumption that  $L=W = j_1 = j_2$ . The solid lines are the results for four individual clusters while the dashed line is for our generalized NFW model. The thick line is the cross-section weighted average for the 200 most massive clusters in our simulations. The lens and source redshifts are taken to be  $z_l = 0.3$  and  $z_s = 1.0$ , respectively.

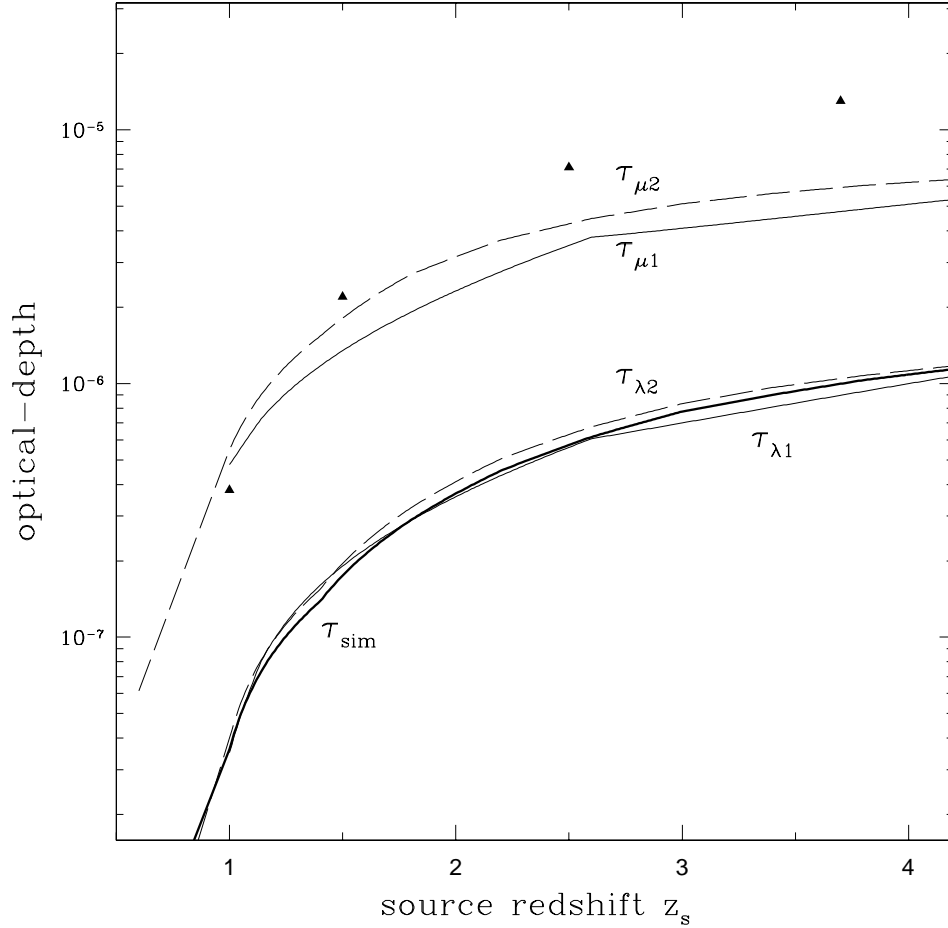


Fig. 6. | The optical depth as a function of the source redshift for giant arcs with  $L=W > 10$ .  $\tau_{\text{sim}}$  is the optical depth calculated using ray-tracing simulations (thick solid line). The thin solid curves labeled  $\tau_{\mu 1}$  and  $\tau_{\lambda 1}$  are those calculated approximating  $L=W$  by the magnification and by the ratio of the two eigenvalues,  $j_1 = \mu j_2$ , respectively. For these curves, the lensing potential includes all the matter distribution within a cube of  $2r_{\text{vir}}$ . The curves labeled  $\tau_{\mu 2}$  and  $\tau_{\lambda 2}$  are for the cases where we calculate the lensing potential including all the particles within a side length of  $4r_{\text{vir}}$  and a projection depth of  $20h^{-1} \text{ Mpc}$ . The triangles are the results of Wandersburg et al. (2004).

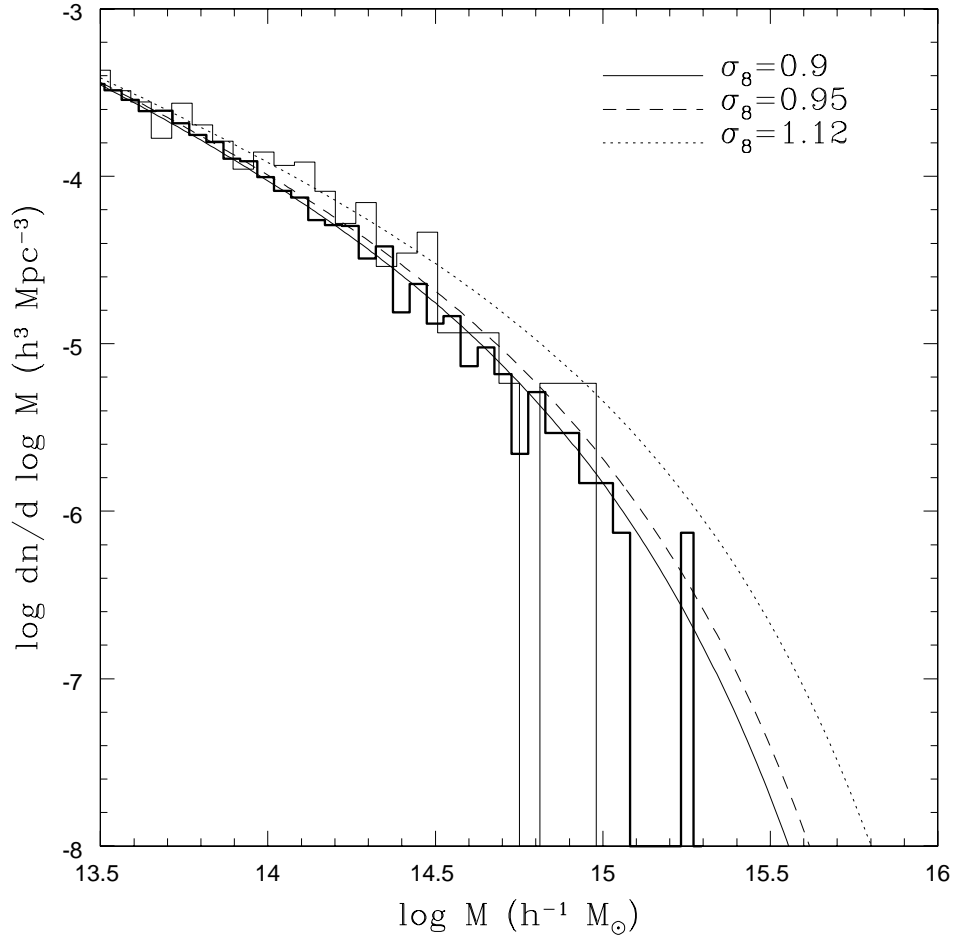


Fig. 7. | The number density of haloes as a function of mass at redshift 0.2 as predicted by the extended Press-Schechter formalism modified by Sheth & Tormann (2002) in the CDM model with different normalizations,  $\sigma_8$ . The solid line is for  $\sigma_8 = 0.9$ , while the dashed and dotted lines are for  $\sigma_8 = 0.95$  and  $\sigma_8 = 1.12$ , respectively. Notice the large differences in the abundance of clusters of galaxies at large masses. The bold histogram shows the mass function for our simulation (for  $\sigma_8 = 0.9$ ) while the thin histogram shows that for the G IF simulation.